Article

# In-situ Imaging of Cysteine in the Brains of Mice with Epilepsy by a Near-infrared Emissive Fluorescent Probe

Songjiao Li, Dan Song, Weijing Huang, Zhen Li, and Zhihong Liu

*Anal. Chem.*, **Just Accepted Manuscript** • DOI: 10.1021/acs.analchem.9b05211 • Publication Date (Web): 06 Jan 2020

# In-situ Imaging of Cysteine in the Brains of Mice with Epilepsy by a Near-infrared Emissive Fluorescent Probe

Songjiao Li, Dan Song, Weijing Huang, Zhen Li*, Zhihong Liu

Key Laboratory of Analytical Chemistry for Biology and Medicine (Ministry of Education), College of Chemistry and Molecular Sciences, Wuhan University, Wuhan, Hubei 430072, China.

**ABSTRACT:** Epilepsy is characterized by oxidative stress in the brain. As the crucial reductive biothiol, cysteine (Cys) directly regulates the occurrence of oxidative stress in the brain. Observations suggest that the decreased cysteine in plasma could potentially serve as a redox biomarker in temporal lobe epilepsy. However, due to the complexity of the brain and lack of appropriate in-situ detecting tools, the concentration change and regulation of Cys in epileptic brains remain unclear. Here, we report a near-infrared imaging probe (named Mito-CP) for tracking endogenous Cys in brains of pentylenetetrazole (PTZ)-induced epileptic seizures with high sensitivity and selectivity. Using this probe, we achieved an in-situ visualization of the increased Cys in PC12 cells under dithiothreitol stimulation. In addition, Mito-CP was able to real-time monitor Cys fluctuation in lipopolysaccharide-mediated oxidative stress in zebrafish. Ultimately, we directly visualized the precipitous reduction of Cys in epileptic brains for the first time. Mito-CP also revealed the fluctuation of Cys in epileptic brains during the treatment by an antiepileptic drug, curcumin. This work provides an effective tool for Cys imaging in brains and will help to expand the understanding of the pathogenesis of epilepsy.

Epilepsy is a brain disorder affecting over 50 million people worldwide and is associated with increased mortality.[1,2] Peripheral biomarkers for epilepsy are notably absent from the tools available to inform its diagnosis and treatment.[3] A growing body of work indicates that epilepsy is characterized by oxidative damage to relevant biological components.[4] Above all, mitochondrial oxidative stress and dysfunction are emerging as key factors that not only result from seizures but may also contribute to epileptogenesis. Mitochondria are the main production source of reactive oxygen species (ROS), and their oxidative damage is a crucial factor in cell death. In order to avoid oxidative stress damage, mitochondria always have a significant number of free radical scavengers, such as cysteine (Cys), which acts as a vital antioxidant reservoir to regulate ROS homeostasis and exerts cytoprotective effect against oxidative damage. Therefore, defining the changes and regulations of Cys is essential for a better understanding of the molecular mechanism underlying epilepsy.[5-7] Whereas current studies on Cys in epilepsy mainly were implemented in plasma.[8] The existing methods cannot reflect Cys level in the brain, especially, they are unable to track native Cys in real-time with spatial resolution during epilepsy. Hence, to explore definitive connections of Cys with epilepsy, it is demanded to develop new tools for in-situ detection of Cys in the brain.

Fluorescence imaging employing small-molecule probes has emerged as a desirable and indispensable tool for interrogating intact living samples.[9-12] Due to the obvious technical and practical advantages of good membrane permeability, high sensitivity, and operational simplicity, fluorescence probes are attracting increasing attention in life science fields. Particularly, NIR excitable probes are considered the most appropriate for brain imaging because they provide a higher signal-to-background ratio, deeper tissue penetration, higher spatial-temporal resolution and less photodamage to biological specimen.[13-16] Recently, some fluorescence probes have been reported for Cys imaging in living cells, zebrafish, and the abdomens of mice.[17-23] However, probes for *in vivo* imaging of Cys in brains has rarely been reported.[24]

Herein, we proposed a novel mitochondria-targeting NIR fluorescent probe (Mito-CP) for in-situ detection of Cys in the brain. (Scheme 1). Mito-CP adopted Mito-Q as the fluorophore and acrylate as the recognition site for Cys. Mito-Q contains an N, N-dimethylamino moiety as an electron donor and a quinoline cation as an electron acceptor. The strong electron push-pull system causes an intramolecular charge transfer (ICT) effect and a Stokes shift of ~260 nm. Such a large Stokes shift can greatly improve the sensitivity by reducing the overlap of excitation and emission bands. The selection of acrylate as the recognition site was to make the probe highly specific to Cys. As known, distinguishing Cys from Hcy and GSH in physiological environments is quite challenging, due to their similar structures and chemical properties. It has been shown that some acrylate-functionalized probes are prone to be more reactive toward Cys over Hcy and GSH.[25,26] Upon a conjugate addition-cyclization reaction of Cys with acrylate and subsequent 1,6-elimination of p-hydroxybenzyl moiety, bright fluorescence of the probe at 700 nm is lighted up. More importantly, Mito-CP possesses efficient blood-brain barrier (BBB) penetrability, which endows the probe with the ability to rapidly enter the brain after intravenous injection and map Cys in the brain. The capability of Mito-CP to detect the variation of Cys, either externally added or generated upon oxidative stress, was demonstrated in varying organisms, including cultured cells, zebrafish, and mice. It was successfully applied to visualize

the fluctuation of Cys in mice brains induced by epileptic seizures and treated with antiepileptic drugs. As far as we know, this is the first in-situ study on the relationship between Cys and epilepsy in brains with a molecular probe.

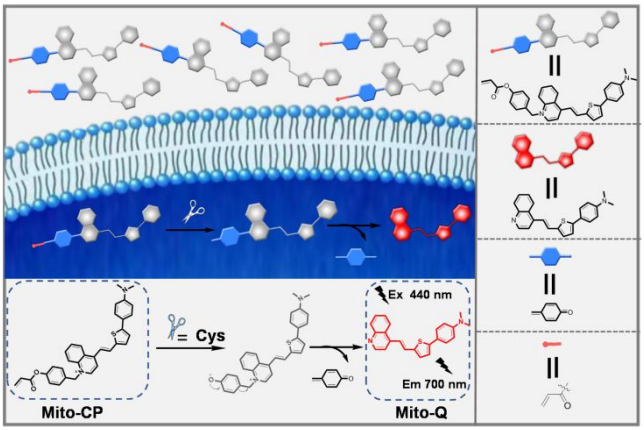


**Scheme 1.** Chemical structure of Mito-CP and proposed reaction mechanisms of Mito-CP toward Cys.

## EXPERIMENTAL SECTION

**Synthesis of Compounds.** A synthetic route for compound Mito-CP from commercially available compounds was provided and depicted in Scheme 2. Compounds 1, 2 and 3 were synthesized according to references.[27,28]

**Synthesis of Mito-Q.** 4-methyl quinoline (160.0 mg, 1.12 mmol) was dissolved in dry DMF (10 mL) and then benzoyl chloride (80.0 mg, 0.56 mmol) was added. The resultant mixture was stirred for 20 minutes at room temperature. After that, Compound 3 (130.0 mg, 0.56 mmol) was added and the solution was refluxed for another 5 hours at 160 °C. When the reaction was completed according to TLC, the reaction mixture was cooled to room temperature, diluted with $H_2O$ and extracted with ethyl acetate for three times. Combined organic layers were washed by saturated sodium thiosulfate solution and dried by anhydrous $Na_2SO_4$. Then the solvent was removed under reduced pressure and the residue was purified by silica gel column chromatography to give the desired product 150 mg. Yield 75%. $^1$H NMR (400 MHz, $CDCl_3$, Figure S1) $\delta$ 8.87 (d, J = 4.0 Hz, 1H), 8.23 (d, J = 8.0 Hz, 1H), 8.13 (d, J = 8.0 Hz, 1H), 7.73 (t, J = 8.0 Hz, 1H), 7.61-7.52 (m, 5H), 7.48 (s, 1H), 7.12 (s, 2H), 6.74 (d, J = 8.0 Hz, 2H), 3.01 (s, 6H). $^{13}$C NMR (101 MHz, $CDCl_3$, Figure S2) $\delta$ 150.3, 150.1, 148.8, 146.3, 142.7, 139.2, 130.1, 129.9, 129.3, 128.2, 126.8, 126.4, 126.2, 123.4, 122.1, 121.4, 120.3, 116.2, 112.4, 40.4. HRMS (Figure S3) m/z: calcd for $C_{23}H_{20}N_2S$ $[M]^+$: 357.142, found: 357.142.

**Synthesis of Probe Mito-CP.** A solution of compound 2 (100.0 mg, 0.42 mmol) and Mito-Q (150.0 mg, 0.42 mmol) were mixed in acetonitrile (5 mL) and then piperidine (0.05 mL) was added to the solution. The reaction mixture was refluxed with stirring. After the reaction was completed, the reaction mixture was cooled to room temperature and solvent was removed under reduced pressure. The resulting residue was purified by column chromatography to give the desired product 133 mg. Yield 53%. $^1$H NMR (400 MHz, DMSO, Figure S4) $\delta$ 9.51 (d, J = 4.0 Hz, 1H), 8.98 (d, J = 8.0 Hz, 1H), 8.52 (t, J = 8.0 Hz, 2H), 8.40 (t, J = 12.0 Hz, 1H), 8.15 (t, J = 8.0 Hz, 1H), 7.96 (t, J = 8.0 Hz, 1H), 7.91 (d, J = 16.0 Hz, 1H), 7.76 (d, J = 4.0 Hz, 1H), 7.63 (d, J = 8.0 Hz, 2H), 7.53 (d, J = 4.0 Hz, 1H), 7.47 (d, J = 8.0 Hz, 2H), 7.23 (d, J = 8.0 Hz, 2H), 6.80 (d, J = 8.0 Hz, 2H), 6.53 (d, J = 16.0 Hz, 1H), 6.42 (dd, J = 8.0 Hz, 1H), 6.24 (s, 2H), 6.16 (d, J = 8.0 Hz, 1H), 3.00 (s, 6H). $^{13}$C NMR (101 MHz, DMSO, Figure S5) $\delta$ 164.5, 153.8, 153.6, 151.2, 147.9, 138.4, 138.1, 137.6, 135.9, 135.6, 134.6, 132.7, 129.4, 128.9, 127.9, 127.4, 126.9, 123.6, 123.4, 123.2, 122.9, 116.7, 116.1, 112.8, 58.7, 51.8. HRMS (Figure S6) m/z: calcd for $C_{33}H_{29}N_2O_2S$ $[M]^+$: 517.194, found: 517.193.

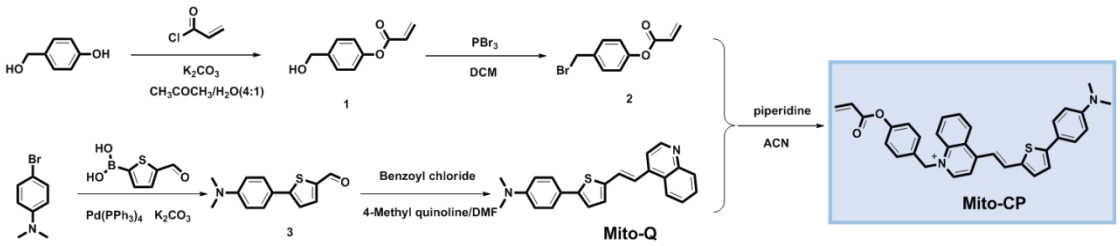


**Scheme 2.** Synthetic route of the probe Mito-CP.

## RESULTS AND DISCUSSION

**Sensing Properties of Mito-CP toward Cys.** The response of Mito-CP to Cys was first investigated in aqueous solutions. Upon the addition of Cys, an increase of fluorescence intensity was observed at 700 nm (Figure 1a). It is worth noting the remarkable Stokes shift of 260 nm, which is larger than that of most NIR emissive fluorescence probes and is in favor of signal/noise ratio of imaging because of the reduction of cross-talk between excitation and emission. Moreover, the UV-vis absorption spectra of Mito-CP with different concentrations of Cys were recorded (Figure 1b). With the Cys amount increased, the absorption peak at 560 nm decreased gradually combined with the emerging of a new absorption peak at 440 nm, which acts as the excitation wavelength of the reaction product (the fluorophore). The fluorescence titration exhibited a maximum enhancement of 12-fold at 100 μM Cys. In addition, a good linearity was obtained over the concentration range of 0.05-10.0 μM for Cys. The regression equation was y = 160.89 + 88.307 × [Cys] with a linear coefficient $R^2$ of 0.993. The limit of detection (LOD, S/N = 3) was calculated as 20.8 nM (Figure 1c), standing for a quite high sensitivity for Cys among all the reported fluorescence probes.

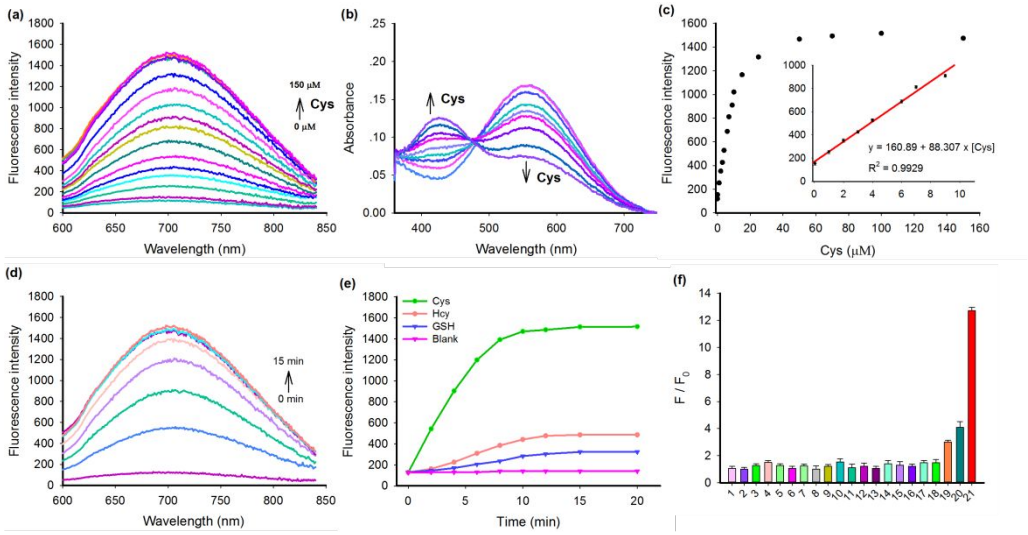


**Figure 1.** (a) Fluorescence spectra of Mito-CP (10 μM) in the presence of different concentrations of Cys (0-150.0 μM); (b) absorption spectra of Mito-CP (10 μM) in the presence of different concentrations of Cys (0-10.0 μM); (c) linear relationship between fluorescence intensity at 700 nm and concentrations of Cys; (d) fluorescence spectral changes of Mito-CP (10 μM) against time in the presence of Cys (100 μM) in DMSO / PBS buffer (3:7, v/v, pH 7.4) at 37 °C; (e) Time-dependent response of Mito-CP (10 μM) to Cys (100 μM), Hcy (100 μM) and GSH (10 μM), respectively; (f) Fluorescence responses of Mito-CP (10 μM) upon addition of amino acids (1. Ala, 2. Glu, 3. Arg, 4. Ser, 5. Lys, 6. Asp, 7. Gly, 8. Leu, 9. Ile, 10. Glu, 11. Tyr, 12. His, 13. Trp, 14. Thr, 15. Phe, 16. Asn, 17. Met, and 18. Val, 100 μM each) and biothiols (19. GSH, 100 μM; 20. Hcy, 100 μM; 21. Cys, 100 μM) in DMSO / PBS buffer (3:7, v/v, pH 7.4) at 37 °C.

Next, the effect of pH on the fluorescence intensity of the probe in absence and presence of Cys was examined. As shown in Figure S7, the probe possessed optimal fluorescence response toward Cys in the physiological pH range (7.0-8.0). The time course studies showed that the fluorescence intensity of the reaction plateaued in approximately 15 min and remained virtually unchanged (Figure 1d). Next, we assessed the specificity of Mito-CP to Cys over other amino acids and thiols (Hcy and GSH) with similar structures. The time-dependent fluorescence responses of probe to the thiols with the same concentration were then monitored. As seen in Figure 1e, as compared to the other thiols, the reaction between Cys and Mito-CP exhibited significantly higher reaction speed and higher fluorescence intensity at a steady-state, suggesting the probe can be used to effectively discriminate Cys from Hcy and GSH. Principally, the high selectivity of probe Mito-CP for Cys over other thiols can be attributed to the kinetic rate of the intramolecular cyclization reactions. The intramolecular cyclization reaction is kinetically favored for Cys to form a seven-membered ring compared to that of Hcy which forms an eight-membered ring. The intramolecular cyclization for GSH is hindered by the bulkiness of its tripeptide; as a result, only the conjugated thioether can be generated. Moreover, other amino acids without thiol did not induce any detectable fluorescence responses (Figure 1f). Other interfering substances such as $H_2S$, metal ions ($K^+$, $Na^+$, $Ca^{2+}$, $Mg^{2+}$), $H_2O_2$, HClO were also investigated. As shown in Figure S8, no response was observed.

To confirm the reaction mechanism, the reaction mixture of Mito-CP and Cys was analyzed by HRMS. After reacting with Cys, the peak at m/z = 517.1933 declined and a new peak at m/z = 357.1422 corresponding to Mito-Q appeared. This verified that probe Mito-CP can be cleaved by Cys to produce Mito-Q. (Figure S9). In order to further evaluate the optical properties of Mito-CP in response to Cys, theoretic calculation by density functional theory (DFT) with the B3LYP/6-31G (d) method was conducted using the Gaussian 09 program. The optimized structures of Mito-CP and Mito-Q are provided in Figure S10. The highest occupied molecular orbital (HOMO) and the lowest unoccupied molecular orbital (LUMO) of Mito-CP and Mito-Q are given in Figure S11. For the cleavable product Mito-Q, the π electrons resides mainly on the N, N-dimethylamino group in the highest occupied molecular orbital (HOMO), whereas the LUMO is mostly located on the quinoline group with a bigger energy gap (5.13 eV) than that of Mito-CP (3.31 eV), which is in good agreement with the apparent blueshift in absorption spectra of Mito-Q compared with that of Mito-CP. All these results validated our design that the reaction of Mito-CP with Cys causes the cleavage of acrylate and subsequent 1,6-elimination of p-hydroxybenzyl moiety to yield Mito-Q.

**Detection of Cys with Mito-CP in live cells.** Standard 3-(4,5-dimethylthiazol-2-yl)-2,5-diphenyltetrazolium bromide (MTT) assay using PC12 cells was performed to assess the cytotoxicity of Mito-CP. A >90% survival rate of cells was maintained even with the Mito-CP concentration as high as 30 μM (Figure S12). To evaluate the performance of Mito-CP in cultured cells, we imaged Cys with Mito-CP in PC12 cells. When the PC12 cells were incubated with Mito-CP, a red fluorescence signal was observed due to the presence of endogenous Cys in cells (Figure 2a). The fluorescence intensity increased gradually with the extension of incubation time and reached the maximum at 30 min (Figure S13). When the PC12 cells were first pretreated with N-ethylmaleimide (NEM, a recognized thiol eliminator[29]) and then with Mito-CP, nearly no fluorescence signal was detected (Figure 2b), indicating that the endogenous Cys was exhausted by NEM. When excess exogenous Cys was introduced into cells after treating with NEM, we again observed strong intracellular

fluorescence (Figure 2c). Conversely, the addition of external Hcy or GSH to the NEM-treated PC12 cells did not cause a detectable fluorescence signal (Figure 2d, e). These imaging phenomena are consistent with the results in solutions, further verifying that the probe Mito-CP can be used to selectively detect Cys in various environments. Dithiothreitol (DTT) is a known stimulus to produce Cys in cells[30]. When the NEM-treated PC12 cells were incubated with DTT, elevated fluorescence was detected (Figure 2f), further confirming the ability of Mito-CP to track the endogenous Cys. Moreover, we administrated the cells with external $H_2O_2$ to imitate intracellular oxidative stress. In this case, much weaker intracellular fluorescence was observed in the cells (Figure 2g, as compared to 2a). The intracellular fluorescence intensities of the above seven groups of cells were calculated and presented in Figure 2h.

To identify the intracellular localization of Mito-CP, we performed fluorescence colocalization experiments employing organelle trackers (Mito-, ER-, and Lyso-Tracker Green). The fluorescence of Mito-CP overlapped well with that of Mito-Tracker (with a Pearson's coefficient (PC) of 0.897) but only partially overlapped with Lyso-Tracker (PC 0.709) or ER-Tracker (PC 0.724), demonstrating that Mito-CP distributes mainly in mitochondria (Figure S14). This can be explained by the charge attraction between Mito-CP with a positive charge and cellular mitochondrial membrane with negative potential.

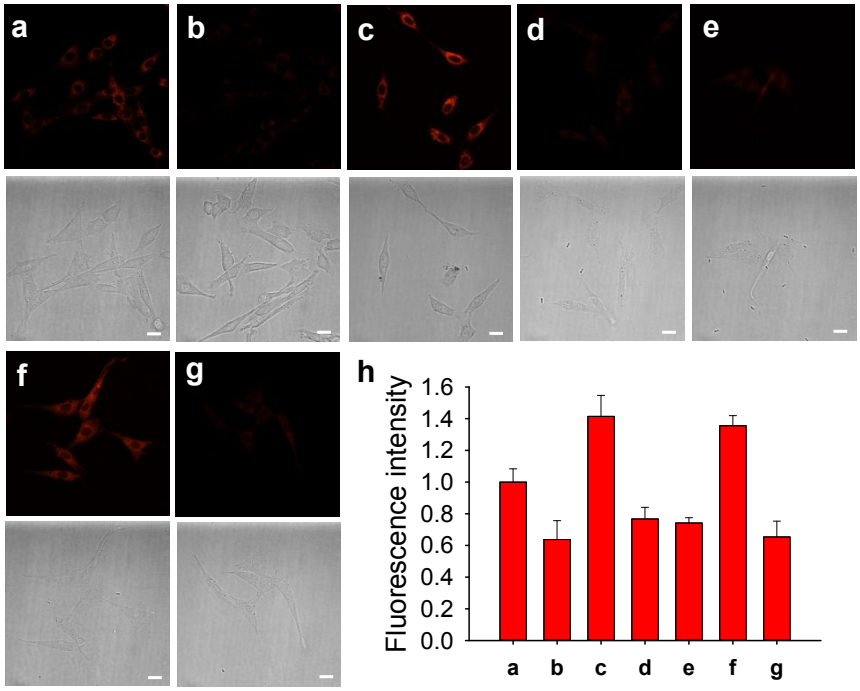


**Figure 2.** Fluorescence images of PC12 cells, pictures below are corresponding bright-field photos. (a) PC12 cells incubated with Mito-CP (10 μM) for 30 min. (b) PC12 cells pretreated with NEM (1.0 mM) for 30 min and then incubated with Mito-CP (10 μM) for 30 min. (c,d,e) PC12 cells pretreated with NEM (1.0 mM) for 30 min and then incubated with Cys, Hcy, and GSH (100 μM) for 30 min, respectively, and finally incubated with Mito-CP (10 μM) for 30 min. (f) PC12 cells pretreated with NEM (1.0 mM) for 30 min and then incubated with DTT (1.0 mM) and then incubated with Mito-CP (10 μM) for 30 min. (g) PC12 cells pretreated with $H_2O_2$ (200 μM) for 30 min and then incubated with Mito-CP (10 μM) for 30 min. (h) Relative pixel intensity of the corresponding fluorescence images in a-g. Scale bar = 10 μm.

**Fluorescence Imaging of Cys in Living Zebrafish under Oxidative Stress.** With the promising imaging performance in live cells in hand, we were interested in investigating the Cys fluctuation under oxidative stress status using zebrafish as a model. Oxidative stress refers to the cellular status with enhanced production of intracellular reactive oxygen species and a decrease of Cys concentration level, which impairs the function of the cellular antioxidant defense system.[31,32] The oxidative stress status of zebrafish was mediated by lipopolysaccharide (LPS) in our experiments, and then the zebrafish were imaged at a set of time points from 30 to 180 min. As shown in Figure 3, clear fluorescence was observed for the control group without LPS administration, but a decrease of fluorescence was observed for the LPS (100 μg/mL) stimulated zebrafish that was co-incubated with Mito-CP. The mean fluorescence intensity of zebrafish declined with time, which was in line with the reduced concentration of Cys in oxidative stress status. Therefore, the probe Mito-CP was demonstrated to be able to image fluctuation of endogenous Cys in living animals.

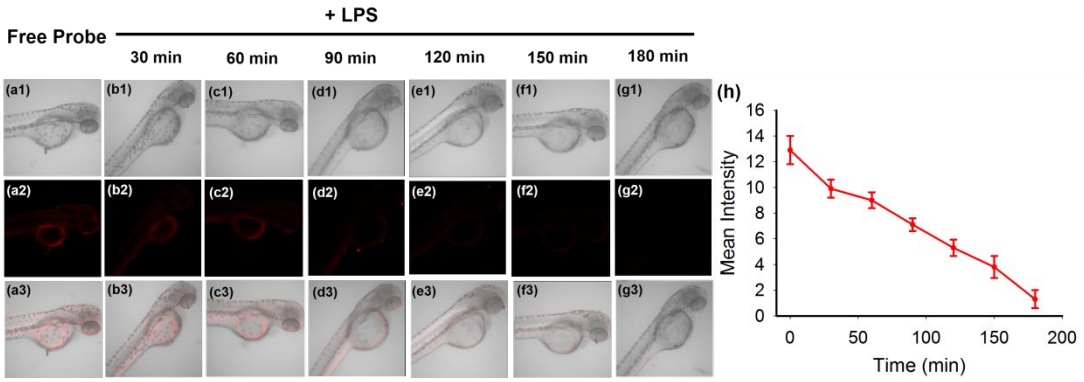


**Figure 3.** Fluorescence images of probe Mito-CP responding to Cys in living 5-day-old zebrafish under oxidative stress status by confocal fluorescence imaging. (a) Zebrafish were incubated with Mito-CP (10 μM, 60 min), and then imaged. (b−g) Zebrafish were mediated by lipopolysaccharide (LPS, 100 μg/mL) for 30 (b), 60 (c), 90 (d), 120 (e), 150 (f), or 180 (g) min, and subsequently incubated with Mito-CP (10 μM) for 60 min, and then imaged. (h) Mean fluorescence intensity of zebrafish shown in (a-g).

**Fluorescence imaging of Cys in the brains of mice.** Since the emission of the probe is in the NIR region, it causes very slight photo-damage to biological samples. In particular, it could penetrate deeper tissues with weak background fluorescence interference. These merits make Mito-CP well suited for *in vivo* imaging applications. Therefore, we exploited *in vivo* fluorescence imaging of Cys with the probe in mice. In order to possibly cross the BBB, the lipophilicity index log P of a molecule probe normally needs to be within the range of 1.0-3.0, with the molecular weight (MW) < 600 Da. The log P value of Mito-CP was calculated as 1.98, fulfilling the criterion of lipophilicity. At the same time, we avoided constructing too large a conjugated system for the red shift of the emission wavelength, so that Mito-CP also possessed an appropriate MW (517 Da). The BBB penetrability of Mito-CP was then experimentally confirmed by ex vivo fluorescence imaging. After intravenous (i.v.) injection of the probe, the fluorescence at 700 nm of various organs were measured and compared. The images of both the entire organs (Figure S15) and their sliced tissues (Figure S16) indicated Mito-CP could reach brains through i.v. injection and achieve ideal images. Besides, the major organs of mice from the control and experiment groups were collected for histological analysis. As shown in Figure S17, there was negligible organ damage (no necrosis, edema, inflammatory infiltration, or hyperplasia) in the sections of the six organs, demonstrating that Mito-CP has good biosafety. To investigate whether Mito-CP can be used for mapping the dynamic changes of Cys *in vivo*, a group of five-week-old BALB/c nude mice were studied with intraperitoneal (i.p.) injection of different agents to induce the changes of endogenous Cys. Images were collected at different time points after intravenous (i.v.) injection of Mito-CP (Figure 4). As displayed in Figure 4a and 4b, a bright fluorescence signal was detected in the control group, which indicates Mito-CP can effectively penetrate the BBB of healthy mice and react with the intrinsic Cys in the brain. Higher fluorescence intensity was observed in the brain region of mice injected with Cys than that in the control sample. In contrast, when the BALB/c nude mice were pretreatment with $H_2O_2$ or NEM, the NIR fluorescence signals in brains were lower than that in the control group. At all the time points tested, i.e., 5, 15, 30, 45, and 60 min, the fluorescence intensity of four sample groups all displayed the same tendency. When fluorescence imaging was carried out on the dissected brains of the four groups, the same result was obtained (Figure 4c). These findings verified that Mito-CP was capable of detecting Cys levels in the brains of living body.

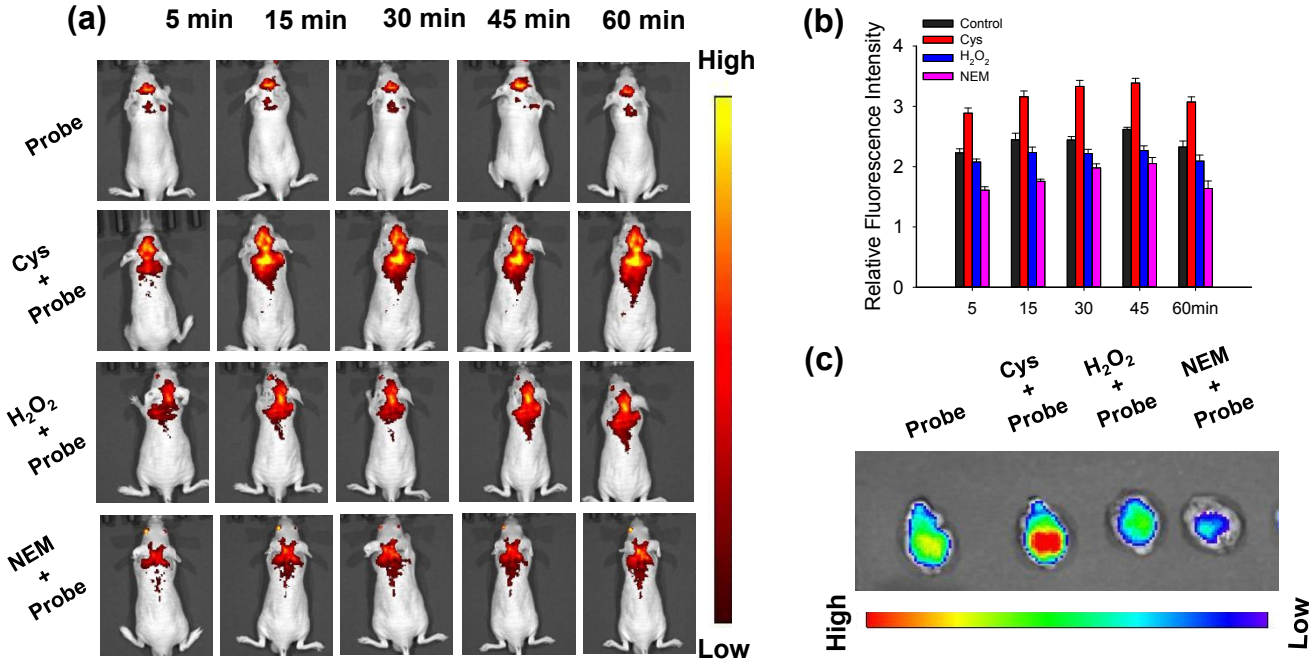


**Figure 4.** (a) Mapping Cys fluxes in live mice with Mito-CP. 5-weeks-old BALB/c nude mice were performed with intraperitoneal (i.p.) injection of different agents. Images were recorded after i.v. injection with Mito-CP at 5, 15, 30, 45, and 60 min. (b) Quantification of fluorescence intensity of images in (a). (c) The Fluorescence images of dissected brain of the four mice.

**Revealing Cys variation in the brains of Epileptic mice.** With the sensitive and specific response of Mito-CP towards Cys established both in vitro and in vivo, we were then encouraged to explore the participation of Cys in the seizure and treatment of epilepsy by drugs in mice. Epilepsy was induced on a mouse model by intraperitoneal injection of pentylenetetrazole (PTZ) into the nude mice (Figure S18). PTZ is a GABAA antagonist commonly used as a convulsant agent, which slowly results in the development of a kindled model of epilepsy when administered repeatedly in a sub-convulsive dose for a specific period of time.[33] All mice samples were intravenously injected with Mito-CP, and fluorescence imaging was performed at different time post injection. As shown in Figure 5a and 5b, the brains of mice with epilepsy showed evident decreased fluorescence intensity compared to those of normal mice as the control, which demonstrates that the probe could visualize the down-regulation of Cys in the epileptic brains. However, when the epileptic mice were treated with the antiepileptic drug curcumin[34-35], the fluorescence in the brain region was restored and close to that of normal mice. The dissected brain of each mouse was also imaged, which showed the same result as that *in vivo* (Figure 5c). Overall, these results provided direct evidence for the negative correlation between Cys levels and epilepsy behaviors. Furthermore, the brain tissue of each group was analyzed by hematoxylin and eosin (H&E) staining (Figure 5d). The normal control group showed a clear hierarchical structure, neatly arranged nerve cells, intact cell membranes and uniform cytoplasmic staining. On the contrary, severe neuronal death, including neuronal loss and disordered arrangement in hippocampal regions particularly in the CA1 and CA3 regions, could be obviously observed after the administration of PTZ. The epileptic and curcumin-treated group presented a similar H&E staining result with the control. These results were in good agreement with the observation of *in vivo* fluorescence imaging.

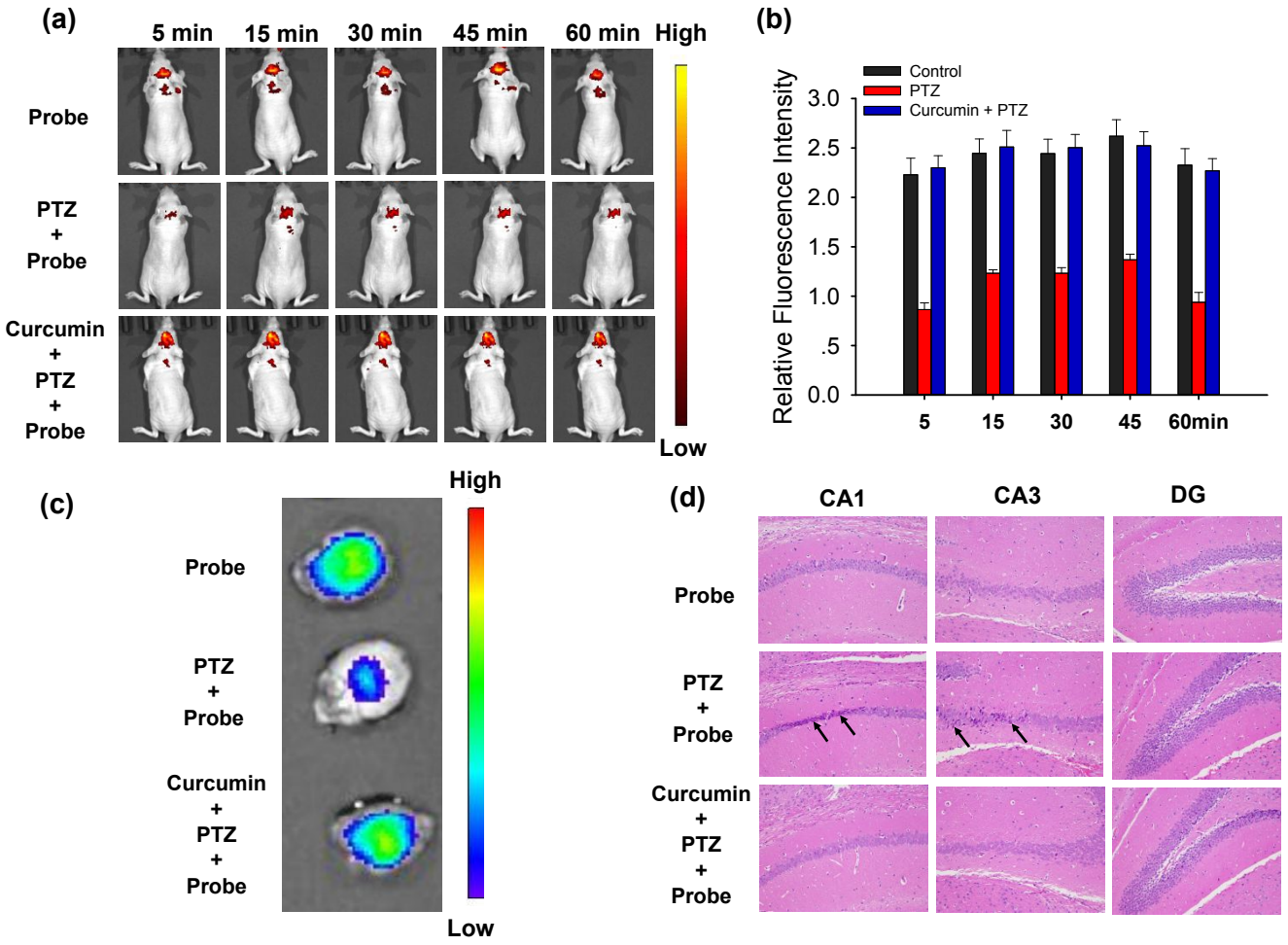


**Figure 5.** (a) *In vivo* NIR fluorescence imaging with Mito-CP. From top to bottom, images of healthy mice, epileptic mice and curcumin-treated epileptic mice at 5, 15, 30, 45, and 60 min after intravenous injection (i.v.) of Mito-CP. (b) Quantification of images in (a). (c) The Fluorescence images of separated brain from the mice. (d) H&E staining for evaluating neuronal damage in the hippocampal region after PTZ administration.

## CONCLUSIONS

In summary, we created a novel NIR emissive fluorescent probe named Mito-CP for the detection of Cys, which possessed high sensitivity and specificity toward Cys. Mito-CP also featured good mitochondria-targeting and BBB penetrating abilities. Using this probe, we achieved in-situ visualization of the Cys variations in live cells and zebrafish with oxidative stress under external stimulation. The NIR emission and large Stokes shift of Mito-CP enabled it to monitor Cys in the brains of live mice. Ultimately, we were able to explore for the first time the participation of Cys during the seizure and treatment of epilepsy on mouse model. Our results provided fresh insight into the relationship between mitochondrial Cys level, an indicator of oxidative stress, and the occurrence, development and treatment of epilepsy.

## ASSOCIATED CONTENT

### Supporting Information

The Supporting Information is available free of charge on the ACS Publications website.

$^{1}$H NMR, $^{13}$C NMR and MS spectra, additional spectroscopic data, cell cytotoxicity and supplemental fluorescence images.

## AUTHOR INFORMATION

### Corresponding Author

*E-mail: zhenli@whu.edu.cn.

### Notes

The authors declare no competing financial interest.

## ACKNOWLEDGMENT

This work was financially supported by the National Natural Science Foundation of China (No. 21575109, 21625503).

## REFERENCES

(1) Dua, T.; De Boer, H. M.; Prilipko, L. L.; Saxena, S. Epilepsy care in the world: results of an ILAE/IBE/WHO global campaign against epilepsy survey. *Epilepsia* **2006**, *47*, 1225-1231.

(2) Löscher, W.; Schmidt, D. Modern antiepileptic drug development has failed to deliver: ways out of the current dilemma. *Epilepsia* **2011**, *52*, 657-678.

(3) Agarwal, N. B.; Agarwal, N. K.; Mediratta, P. K.; Sharma, K. K. Effect of lamotrigine, oxcarbazepine and topiramate on cognitive functions and oxidative stress in PTZ-kindled mice. *Seizure* **2011**, *20*, 257-262.

(4) Patel, M. Mitochondrial dysfunction and oxidative stress: cause and consequence of epileptic seizures. *Free Radic. Biol. Med.* **2004**, *37*, 1951-1962.

(5) Stobiecka, M.; Deeb, J.; Hepel, M. Ligand exchange effects in gold nanoparticle assembly induced by oxidative stress biomarkers: Homocysteine and cysteine. *Biophys. Chem*. **2010**, *146*, 98-107.

(6) Stipanuk, M. H. Sulfur amino acid metabolism: pathways for production and removal of homocysteine and cysteine. *Annu. Rev. Nutr*. **2004**, *24*, 539-577.

(7) Kimura, Y.; Kimura, H. Hydrogen sulfide protects neurons from oxidative stress. *Faseb J*. **2004**, *18*, 1165-1167.

(8) Liang, L. P.; Patel, M. Plasma cysteine/cystine redox couple disruption in animal models of temporal lobe epilepsy. *Redox Biol*. **2016**, *9*, 45-49.

(9) Xu, S.; Liu, H. W.; Yin, X.; Yuan, L.; Huan, S. Y.; Zhang, X. B. A cell membrane-anchored fluorescent probe for monitoring carbon monoxide release from living cells. *Chem. Sci*. **2019**, *10*, 320-325.

(10) Li, P.; Wang, J.; Wang, X.; Ding, Q.; Bai, X.; Zhang, Y.; Tang, B. In situ visualization of ozone in the brains of mice with depression phenotypes by using a new near-infrared fluorescence probe. *Chem. Sci.* **2019**, *10*, 2805-2810.

(11) Wang, X.; Li, P.; Ding, Q.; Wu, C.; Zhang, W.; Tang, B. Observation of acetylcholinesterase in stress-induced depression phenotypes by two-photon fluorescence imaging in the mouse brain. *J. Am. Chem. Soc*. **2019**, *141*, 2061-2068.

(12) Li, X.; Gao, X.; Shi, W.; Ma, H. Design strategies for water-soluble small molecular chromogenic and fluorogenic probes. *Chem. Rev*. **2013**, *114*, 590-659.

(13) Liu, Y.; Teng, L.; Chen, L.; Ma, H.; Liu, H. W.; Zhang, X. B. Engineering of a near-infrared fluorescent probe for real-time simultaneous visualization of intracellular hypoxia and induced mitophagy. *Chem. Sci.* **2018**, *9*, 5347-5353.

(14) Cheng, D.; Peng, J.; Lv, Y.; Su, D.; Liu, D.; Chen, M.; Zhang, X. De novo design of chemical stability near-infrared molecular probes for high-fidelity hepatotoxicity evaluation in vivo. *J. Am. Chem. Soc.* **2019**, *141*, 6352-6361.

(15) He, N.; Bai, S.; Huang, Y.; Xing, Y.; Chen, L.; Yu, F.; Lv, C. Evaluation of glutathione S-transferase inhibition effects on idiopathic pulmonary fibrosis therapy with a near-infrared fluorescent probe in cell and mice models. *Anal. Chem*. **2019**, *91*, 5424-5432.

(16) Tian, Y.; Li, Y.; Jiang, W. L.; Zhou, D. Y.; Fei, J.; Li, C. Y. In-situ imaging of azoreductase activity in the acute and chronic ulcerative colitis mice by a near-infrared fluorescent probe. *Anal. Chem.* **2019**, *91*, 10901-10907.

(17) Wang, B. J.; Liu, R. J.; Fang, J.; Wang, Y. W.; Peng, Y. A water-soluble dual-site fluorescent probe for the rapid detection of cysteine with high sensitivity and specificity. *Chem. Commun*. **2019**, *55*, 11762-11765.

(18) Yang, M.; Fan, J.; Sun, W.; Du, J.; Peng, X. Mitochondria-anchored colorimetric and ratiometric fluorescent chemosensor for visualizing cysteine/homocysteine in living cells and daphnia magna model. *Anal. Chem.* **2019**, *91*, 12531-12537.

(19) He, L.; Yang, X.; Xu, K.; Lin, W. Improved aromatic substitution–rearrangement-based ratiometric fluorescent cysteine-specific probe and its application of real-time imaging under oxidative stress in living zebrafish. *Anal. Chem.* **2017**, *89*, 9567-9573.

(20) Dong, B.; Lu, Y.; Zhang, N.; Song, W.; Lin, W. Ratiometric imaging of cysteine level changes in endoplasmic reticulum during $H_2O_2$-induced redox imbalance. *Anal. Chem*. **2019**, *91*, 5513-5516

(21) Qi, Y.; Huang, Y.; Li, B.; Zeng, F.; Wu, S. Real-time monitoring of endogenous cysteine levels in vivo by near-infrared turn-on fluorescent probe with large stokes shift. *Anal. Chem*. **2017**, *90*, 1014-1020.

(22) Huang, Y.; Zhou, Q.; Feng, Y.; Zhang, W.; Fang, G.; Fang, M.; Meng, X. Rational design of a ratiometric two-photon fluorescent probe for real-time visualization of apoptosis. *Chem. Commun*. **2018**, *54*, 10495-10498.

(23) Huang, Y.; Ren, Q.; Li, S.; Feng, Y.; Zhang, W.; Fang, G.; Meng, X. A dual-emission two-photon fluorescent probe for specific-cysteine imaging in lysosomes and in vivo. *Sens. Actuators B* **2019**, *293*, 247-255.

(24) Zhang, Y.; Wang, X.; Bai, X.; Li, P.; Su, D.; Zhang, W.; Tang, B. Highly Specific Cys Fluorescence probe for living mouse brain imaging via evading reaction with other biothiols. *Anal. Chem.* **2019**, *91*, 8591-8594.

(25) Han, C.; Yang, H.; Chen, M.; Su, Q.; Feng, W.; Li, F. Mitochondria-targeted near-infrared fluorescent off–on probe for selective detection of cysteine in living cells and in vivo. *ACS Appl. Mater. Interfaces* **2015**, *7*, 27968-27975.

(26) Niu, W.; Guo, L.; Li, Y.; Shuang, S.; Dong, C.; Wong, M. S. Highly selective two-photon fluorescent probe for ratiometric sensing and imaging cysteine in mitochondria. *Anal. Chem*. **2016**, *88*, 1908-1914.

(27) Sarkar, A. R.; Heo, C. H.; Kim, E.; Lee, H. W.; Singh, H.; Kim, J. J.; Kim, H. M. A cysteamine-selective two-photon fluorescent probe for ratiometric bioimaging. *Chem. Commun*. **2015**, *51*, 2407-2410.

(28) Fu, W.; Yan, C.; Guo, Z.; Zhang, J.; Zhang, H.; Tian, H.; Zhu, W. H. Rational design of near-infrared aggregation-induced-emission-active probes: in situ mapping of amyloid-β plaques with ultrasensitivity and high-fidelity. *J. Am. Chem. Soc*. **2019**, *141*, 3171-3177.

(29) Yellaturu, C. R.; Bhanoori, M.; Neeli, I.; Rao, G. N. N-Ethylmaleimide inhibits platelet-derived growth factor BB-stimulated Akt phosphorylation via activation of protein phosphatase 2A. *J. Biol. Chem.* **2002**, *277*, 40148-40155.

(30) Balhorn, R.; Corzett, M.; Mazrimas, J.; Watkins, B. Identification of bull protamine disulfides. *Biochemistry* **1991**, *30*, 175-81.

(31) Buttke, T. M.; Sandstrom, P. A. Oxidative stress as a mediator of apoptosis. *Immunol. Today* **1994**, *15*, 7-10.

(32) Iyer, S. S.; Jones, D. P.; Brigham, K. L.; Rojas, M. Am. Oxidation of plasma cysteine/cystine redox state in endotoxin-induced lung injury. *J. Respir. Cell Mol. Biol*. **2009**, *40*, 90-98.

(33) Obay, B. D.; Taşdemir, E.; Tümer, C.; Bilgin, H. M.; Atmaca, M. Dose dependent effects of ghrelin on pentylenetetrazole-induced oxidative stress in a rat seizure model. *Peptides* **2008**, *29*, 448-455.

(34) Reeta, K. H.; Mehla, J.; Gupta, Y. K. Curcumin is protective against phenytoin-induced cognitive impairment and oxidative stress in rats. *Brain Res*. **2009**, *1301*, 52-60.

(35) Mehla, J.; Reeta, K. H.; Gupta, P.; Gupta, Y. K. Protective effect of curcumin against seizures and cognitive impairment in a pentylenetetrazole-kindled epileptic rat model. *Life Sci*. **2010**, *87*, 596-603.

**for TOC only**